

Muon Capture in Hydrogen*

J. E. ROTHBERG,[†] E. W. ANDERSON, E. J. BLESER,[‡] L. M. LEDERMAN,
S. L. MEYER, J. L. ROSEN, AND I-T. WANG

Columbia University, New York, New York

(Received 31 July 1963)

An experiment to measure the muon capture rate in liquid hydrogen was carried out using scintillation counter techniques. The experiment tests muon-electron universality in the weak interaction with a proton at a momentum transfer of 100 MeV/c. The use of ultrapure liquid hydrogen, a purified muon beam, and neutron-gamma ray discriminating detectors made possible the detection of the 5.2-MeV neutron from the relatively improbable capture reaction ($\mu^- + p \rightarrow n + \nu$). Observation of the well-known pion capture reaction ($\pi^- + p \rightarrow n + \gamma$) served as a check on many aspects of the experimental arrangement as well as on the neutron detector efficiency calculation. Several internal checks confirm that impurity captures were negligible. The muon capture rate in the $(p\mu)^+$ ortho molecular state was obtained. The muon molecular formation rate was measured in an independent experiment, but the present result is relatively insensitive to it. The stability of the ortho state against transition to the para ground state for times comparable to the free muon lifetime is confirmed. The experimental result of $464 \pm 42 \text{ sec}^{-1}$ is to be compared with 562 sec^{-1} , the rate expected on the basis of muon-electron universality, the conserved vector current theory, the calculated value of the induced pseudoscalar coupling, and the axial vector and vector coupling constants as determined in the β -decay interaction.

I. INTRODUCTION

A. Status of the Universal Fermi Interaction

THE concept of a universal Fermi interaction (UFI) governing all weak processes was placed on a quantitative foundation by the discovery that the rate of O^{14} beta decay could be used to predict the muon decay rate rather accurately.¹ It is of great interest to test this hypothesis in the case of the muon-proton weak interaction.

The muon-proton interaction at low energies is available for study in nuclear muon capture. This capture can take place because negative muons stopping in matter will eventually cascade to the lowest Bohr orbit of a muonic atom,² a structure that is more tightly bound than a normal atom because of the large muon mass ($m_\mu = 207 m_e$). The atomic wave-function overlap is sufficiently large to make the muon capture interaction competitive with the free muon decay. Most muon capture experiments carried out with complex nuclei have as a prerequisite detailed knowledge of the nuclear wavefunctions, if accurate inferences about the muon-proton coupling constants are to be made.³ Experiments were initiated to study muon capture in hydrogen, a system free of nuclear complications, to provide a test of the universality of the $V-A$ weak interaction coupling theory.

* Work supported in part by the Office of Naval Research.

[†] Present address: Yale University, New Haven, Connecticut.

[‡] Present address: Brookhaven National Laboratory, Upton, New York.

¹ R. P. Feynman and M. Gell-Mann, *Phys. Rev.* **109**, 193 (1958).

² Ya. B. Zel'dovich and S. S. Gershtein, *Usp. Fiz. Nauk* **71**, 581 (1960) [translation: *Soviet Physics—Usp.* **3**, 593 (1961)]; S. Cohen, D. L. Judd, and R. J. Riddell, Jr., *Phys. Rev.* **119**, 384 (1960).

³ R. Klein and L. Wolfenstein, *Phys. Rev. Letters* **9**, 408 (1962); V. L. Telegdi, *Proceedings of the 1960 Annual International Conference on High Energy Physics at Rochester* (Interscience Publishers, Inc., New York, 1960), p. 713; L. Wolfenstein, *ibid.*, p. 529; J. R. Luylen, H. P. Rood, and H. Tolhock, *Nucl. Phys.* **41**, 236 (1963). See also Ref. 6.

Previous experiments on muon capture in hydrogen have established the presence of a strong vector contribution and its sign relative to the axial vector coupling.^{4,5}

B. Experimental Problems in Muon Capture in Hydrogen

1. Specification of the Initial State

A muon-proton coupling scheme of the form vector minus axial vector ($V-A$) results in a strong spin dependence of the muon capture reaction⁶

$$\mu^- + p \rightarrow n + \nu. \quad (1)$$

The possibility of a spin-dependent reaction rate makes accurate specification of the initial muon-proton state vital to an interpretation of experimental results. The history of a negative muon² after considerable re-

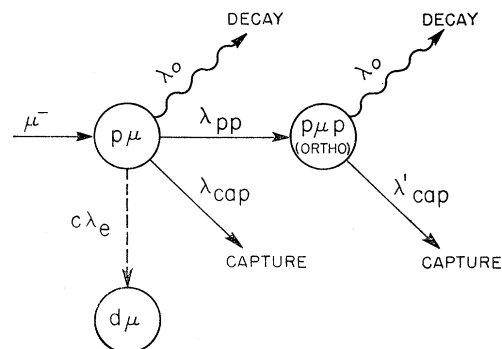


FIG. 1. The history of a muon after coming to rest in pure liquid hydrogen. λ_0 is the free muon decay rate, λ_{cap} is the muon capture rate in the μp atom, λ'_{cap} is the molecular capture rate. When a small amount of deuterium is present (concentration c) then the process indicated by a dashed line can occur.

⁴ R. H. Hildebrand, *Phys. Rev. Letters* **8**, 34 (1962).

⁵ E. Bleser, L. Lederman, J. Rosen, J. Rothberg, and E. Zavattini, *Phys. Rev. Letters* **8**, 288 (1962).

⁶ H. Primakoff, *Revs. Mod. Phys.* **31**, 802 (1959).

duction of velocity in liquid hydrogen (density=0.07 g/cc) proceeds as follows (see Fig. 1). At a low velocity the muon is captured by a proton and cascades to the $1s$ state in less than 10^{-9} sec, this neutral (μp) atomic system is formed in a statistical mixture of triplet and singlet states. It is able to wander through the hydrogen, the muon being exchanged from proton to proton. The result of these exchanges is a 100% population of the energetically lower singlet state and total depolarization of the muons. If even small amounts of deuterium or other atoms are present, then an irreversible transfer to the deuteron (or heavier atom) is likely. The reduced mass effect makes the (μd) system more tightly bound by 130 eV. In pure liquid hydrogen the singlet (μp) system will eventually (in about 0.5 μ sec) become part of a $(p\mu p)^+$ molecular ion^{7,8} if the muon has not decayed first (with lifetime 2.2 μ sec).

It is from the stable molecular ion that the muon is most likely to be captured or to decay. In this experiment the time of each capture event is measured, and thus the configuration from which capture takes place is also known. Only capture events which have originated in a $(p\mu p)$ system have been included in the analysis. There are two questions concerning the nature of the molecular ion which must be considered and which have been answered by detailed calculations: (1) What is the angular momentum character of the molecular ion and, hence, what is the composition in terms of singlet and triplet (μp) ? (2) What is the wave function overlap of the muon and proton?

The $(p\mu p)^+$ molecular ion is almost invariably formed in the ortho state^{2,9} (para formation is $\lesssim 10^{-3}$ smaller) and it has been shown with a high degree of confidence that only states with total spin= $\frac{1}{2}$ are present¹⁰; it then follows that the capture rate from the molecular ion is given by $2\gamma_0(\frac{3}{4}\lambda_s + \frac{1}{4}\lambda_t)$, where λ refers to the capture rate in the triplet and singlet atoms, and $2\gamma_0$ is a wave-function overlap factor (times πa_μ^3) for the ortho molecule. Although the para state is the molecular ion ground state, it can be shown that transitions to it are extremely unlikely during the muon lifetime.^{2,9} The capture rate in this state is expected to be lower, however, being given by $2\gamma_p(\frac{1}{4}\lambda_s + \frac{3}{4}\lambda_t)$, and any appreciable amount of conversion to it could be detected by the experiment.

2. Detection of Capture Events

On the basis of the $V-A$ interaction with certain correction terms included, the rate of Reaction (1) when the muon is bound in the molecular ion is predicted⁶ to be about 560 sec^{-1} . The decay of the muon,

$$\mu^- \rightarrow e^- + \nu + \bar{\nu}, \quad (2)$$

⁷ E. Bleser, L. Lederman, J. Rosen, J. Rothberg, and E. Zavattini, Phys. Rev. Letters 8, 128 (1962); E. Bleser, E. W. Anderson, L. M. Lederman, S. L. Meyer, J. L. Rosen, J. E. Rothberg, and I-T. Wang, Phys. Rev. 132, 2679 (1963).

⁸ G. Conforto, S. Focardi, C. Rubbia, and E. Zavattini, Phys. Rev. Letters 9, 432 (1962).

⁹ S. Weinberg, Phys. Rev. Letters 4, 575 (1960).

¹⁰ A. Halpern and N. Kroll (private communication).

which is not appreciably affected by the muon being bound in a hydrogen orbit (binding energy=2.5 keV) takes place at the rate¹¹ $0.455 \times 10^6 \text{ sec}^{-1}$, so capture is only 1/1000 as likely as decay.

The only signature of a muon capture event is the detection of the 5.2-MeV neutron in Reaction (1). The experimental arrangement for measuring the muon capture rate must be able to distinguish this neutron from all background and must detect it with known efficiency relative to the number of available muons. Because of the possibility of transfer of a muon to deuterium or other impurities in the hydrogen the experiment must be carried out under ultra-pure conditions. The bremsstrahlung of decay electrons [Reaction (2)] constituted an intense source of neutral background which could not be eliminated by shielding. The neutron detectors were capable of distinguishing between neutrons and gamma rays, thus eliminating much of the background.

The known rate of the pion capture reaction

$$\pi^- + p \rightarrow n + \gamma \quad (3)$$

emitting an 8.9-MeV neutron made it possible to perform a control experiment *in situ*.

Experiments on muon capture using hydrogen bubble chamber techniques suffer from uncertainty as to the initial muon state, as well as from an inability to achieve the ultimate in hydrogen purity. On the other hand, the knowledge of kinematics of each event results in better neutron energy resolution than is possible in the present experiment. Scintillation counter techniques are capable of providing data of high statistical accuracy. The experiment to be described here is an extension and refinement of a previous experiment performed at this laboratory.⁵

II. EXPERIMENT

A. Target

Because of the possibility that a muon in the ground state of a μp atom may be transferred to an impurity of higher atomic number, it is essential to carry out the muon capture experiment in ultra-pure hydrogen. The transfer rate to impurities, such as nitrogen, is $\sim 5 \times 10^{10} \text{ sec}^{-1}$ (several times that to deuterium); therefore, a concentration of one part per million would result in 2.5% of the muons ending up bound to the impurity atom. Since the muon capture rates are much larger in impurities than in hydrogen, the effect would be serious. It is clear that extraordinary precautions with the purity of the hydrogen must be taken, such that impurities should constitute less than one part in 10^8 of the hydrogen. The presence of deuterium cannot be tolerated at concentrations greater than a few parts per million. Isotopically pure hydrogen¹² was purified at the entrance to the hydrogen target by passing it into a heated palladium

¹¹ S. L. Meyer, E. W. Anderson, E. Bleser, L. M. Lederman, J. Rosen, J. Rothberg, and I-T. Wang, Phys. Rev. 132, 2693 (1963).

¹² Purchased from L'Air Liquide, Paris.

coil. Only hydrogen forms the appropriate chemical bond with palladium which allows it to diffuse through the walls; other gases do not penetrate the coil and are eliminated. Further purification is obtained by passage of the filtered gas through a cold trap at $\sim 30^\circ\text{K}$. This purification system was subjected to a series of stringent tests. In a test for nitrogen transmission the system following the palladium purifier was evacuated; nitrogen under pressure was admitted to the input end of the palladium coil and the output pressure was watched. No change in pressure was detected, implying a maximum leak through the palladium of 1 part nitrogen to 10^8 parts hydrogen under equal pressure conditions.

{*Note added in proof.* A recent measurement [J. R. Young, *Rev. Sci. Instr.* **34**, 891 (1963)] finds an impurity content of a few parts in 10^{10} for hydrogen permeating Pd.}

The low temperature of the liquid hydrogen (20.4°K) chosen as the target material strongly inhibits the outgassing of foreign materials from the walls of its container. The gas phase was purified and then liquefied within the target itself; this was accomplished by keeping the target region closed and in thermal contact with a reservoir of normal liquid hydrogen. At a very slight pressure above atmospheric, the gas entering from the purification system was liquefied in the previously evacuated target volume (see Fig. 2). The filling procedure took approximately 20 hours during which time the normal liquid hydrogen, absorbing the heat of condensation, was frequently replenished. Once the target was full, heat losses were quite small. The target remained full for several weeks with no deterioration in purity, and required no maintenance except for refilling of the liquid-hydrogen and liquid-nitrogen reservoirs.

Before filling, the "pure system" was evacuated to a pressure of 10^{-6} Torr and baked for several days to release materials adsorbed on the walls. An ion pump backed by a cryogenic adsorption pump was used to evacuate the system. An oil diffusion pump was not used because of the possibility that carbon and carbon compounds might contaminate the target volume.

The ultimate purity of the hydrogen is determined by the residual gas in the target after it has been evacuated to 8×10^{-7} Torr, the impurities introduced through the

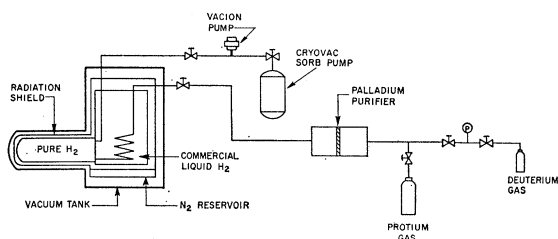


FIG. 2. A diagram of the hydrogen target and associated purification system. The deuterium is used in the experiment to measure molecular constants.

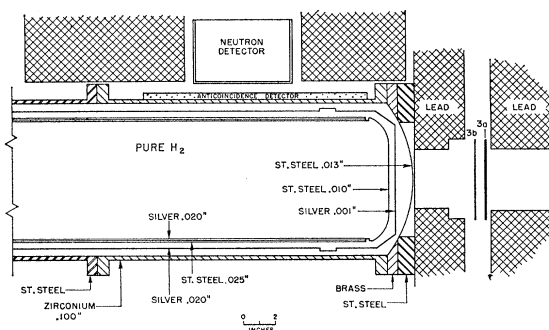


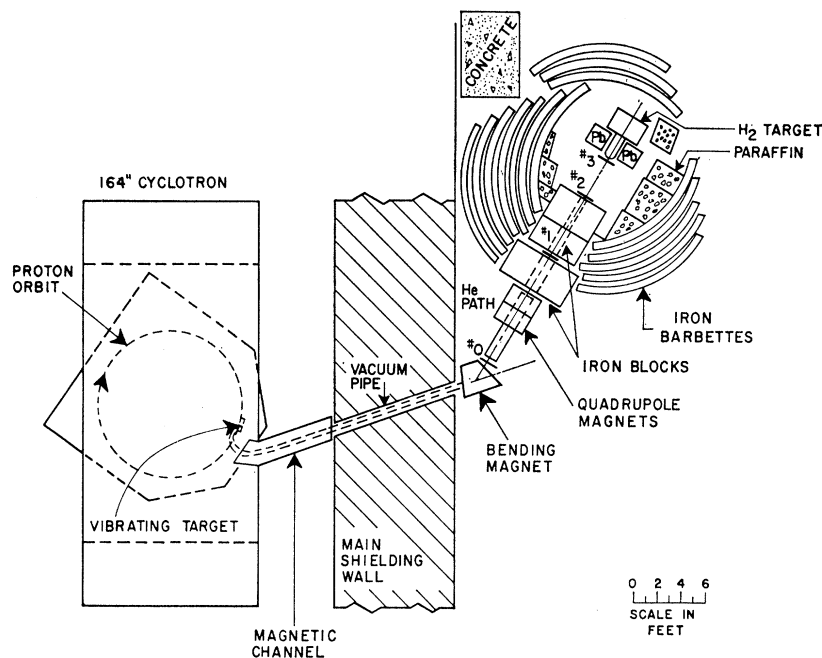
FIG. 3. The hydrogen target and local shielding showing locations of detectors.

palladium, degassing from the walls during the several weeks of running, and leaks in the system. The first consideration gives an impurity concentration of less than 10^{-11} as does the second. The observed leak-up rate at room temperature of 10^{-4} Torr per day projects to an impurity concentration of 10^{-8} in 10 days. If this leak-up rate is due principally to wall degassing, it becomes quite negligible at liquid-hydrogen temperatures. No leak-up rate could be observed for the target at liquid-hydrogen temperatures, since its vacuum was better than that of the pumping manifold. A further check is provided by the neutron yield which showed no detectable increase during the course of the run (see Table II). This establishes an upper limit on the effect of any possible leak-induced impurities of the order of one-half the final error quoted.¹³

Aside from structural consideration, the primary requirements in the target design were that it be constructed exclusively of elements with high atomic number to minimize the effect of muons which might stop in the target walls. In the case of iron, for example, the muon lifetime in the atomic ground state is $0.2 \mu\text{sec}$, as compared to $2.2 \mu\text{sec}$ in hydrogen, so that one has only to delay event acceptance for about $1.0 \mu\text{sec}$ after which time the entire effect of wall captures has disappeared. The inner hydrogen target was constructed of stainless steel for mechanical strength and was lined with silver to provide a very high Z barrier for muons headed toward the walls. A silver thermal radiation shield held at liquid-nitrogen temperature was suspended inside the vacuum jacket whose outer wall was fabricated of zirconium. Figure 3 shows the thickness and location of the target walls and window. The target window through which the muon beam enters was made as thin as safety permitted in order to decrease the number of muons stopping in it and, more important, to minimize multiple scattering of the beam which would increase the likelihood of wall captures in the vicinity of the neutron detectors.

¹³ An increase in neutron yield was observed during an independent run in which deuterium was being added to the target system. This was traced to a leak in the exhaust valve.

FIG. 4. Cyclotron floor plan showing shielded "house" and beam detectors.



B. Measurement of Molecular Constants

Using the same hydrogen target and beam conditions, an experiment was performed to measure several molecular constants as well as (pd) fusion parameters.⁸ The measurement of λ_{pp} , the (μp) to $(p\mu p)$ conversion rate, was of greatest interest to the present experiment.

C. Muon Beam and Geometrical Arrangement

For the purpose of this experiment a muon beam with pion and electron contamination was considered unsatisfactory. First, pions stopping in the vicinity of the hydrogen target would produce neutron background; second, electrons in the beam would enter the target with the muons and might make an accurate determination of the number of muons stopping in the hydrogen difficult; they would also increase the number of accidental delayed "muon"-neutron coincidences.

Since the source of muons is more diffuse than that of pions and electrons it is possible, by suitable adjustment of the bending magnet current outside the shielding wall, to focus magnetically off the meson target and reduce greatly the transmission of the unwanted particles while decreasing the number of muons in the beam by less than a factor of 2. Searches for the optimum conditions for this purified beam were undertaken, using a time-of-flight system.¹⁴ Two scintillation counters (No. 0 and No. 2) employing 56AVP photomultipliers were placed about 6 m apart (see Fig. 4); the output pulses from these were used as the start and stop pulses in a $\frac{1}{4}$ nsec resolution time-to-height converter

¹⁴ The time-to-height converter as well as the logic modules used in the experiment were designed for general laboratory use by W. LeCroy.

whose output was displayed in a 100-channel pulse analyzer. At the particle momenta of interest (about 120 MeV/c) the pions and muons could be easily resolved. The mass spectrum that was obtained in this way was checked from time to time by measuring the differential stopping rate of the beam as a function of moderator thickness. The working conditions that were finally chosen involved an increase in bending magnet current to select muons of 128 MeV/c. This momentum is about 15% higher than the momentum of the majority of the pions which are normally transmitted through the shielding wall. Under these conditions less than 2% of the beam particles were pions and electrons. Figure 5 shows the mass spectrum of the beam consisting of pions, muon, and electrons as the purification is improved.

A 128-MeV/c muon beam was bent through 41° by a wedge-shaped dipole magnet. The beam then passed through a pair of quadrupole magnets which were set to focus the beam within the hydrogen target (see Fig. 4).

A beryllium moderator was used to reduce the muon energy from the initial 60 MeV to an energy which would allow muons to stop between the neutron detectors at the center of the target (see Figs. 3 and 4). Beryllium was chosen in order to reduce multiple scattering of the beam. Muons with a mean energy of 26 MeV impinged on the window of the target and entered the hydrogen with 24.5 MeV.

Two different beam collimator arrangements were used during two successive weeks of data taking. The principal difference was in the aperture diameter. The two geometrical arrangements will be referred to as the

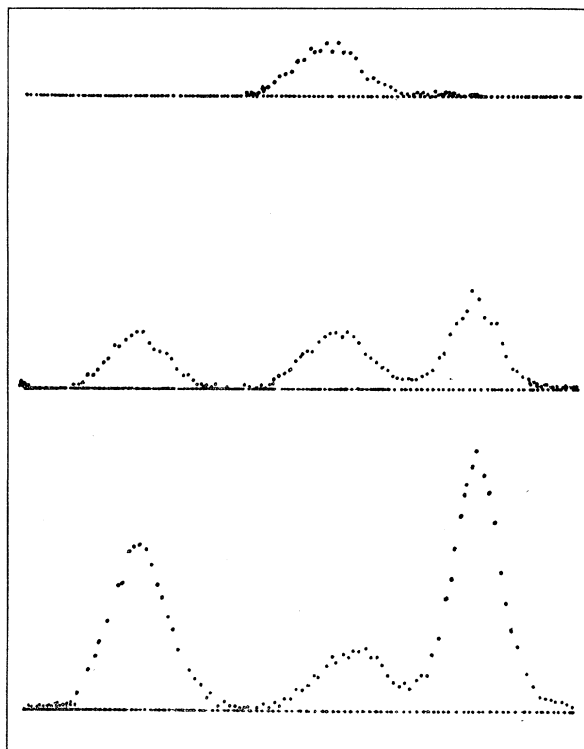


FIG. 5. Pulse-height distribution of time-to-height converter output. Beam particles traverse a 6-m flight path. Lowest curve shows the unpurified beam with electrons on the left, muons, then pions. Upper curve represents the purified muon beam used in the experiment.

“4-in.” and the “3-in.” conditions, respectively. Although the latter reduced the number of muons entering the target, a somewhat improved ratio of wall stopping muons to hydrogen stopping muons was observed. The data from these two independent runs were analyzed separately and showed no significant difference. This is strong confirmation that correct account was made of phenomena relating to wall stoppings and wall penetration. Figure 4 shows the location of the beam detectors with respect to the shielding arrangement. When the purified muon beam is used, the pions are of lower momentum than the muons which are accepted by the collimator system. They are, therefore, bent through a larger angle and most of them strike the shielding blocks or the sides of collimator walls. The location of counter No. 1 was chosen so as to detect those pions which were likely to give rise to a detected neutron. These events were discarded, reducing the accidental neutron rate substantially.

Counters No. 3a and No. 3b were located adjacent to one another downstream of the moderator. The second of the two was made extremely thin (0.020 in.) in order to reduce the number of muons stopping in plastic to a tolerable level. The two counters were placed in coincidence with one another so as to reduce the accidental counting rate in the beam telescope. Without No. 3a an accidental coincidence in this case would very

likely be due to a muon stopping in the beryllium moderator coincident with a noise pulse in No. 3b, and would be electronically indistinguishable from a hydrogen stopping.

D. Electron and Neutron Detectors

The hydrogen target was surrounded by four $11\frac{1}{2} \times 14 \times \frac{3}{8}$ -in. plastic scintillation counters; behind each of these was mounted a neutron detector surrounded by at least 2 in. of lead on five of its sides. The thin counters were labeled $A_1, A_2, A_3,$ and A_4 , and the respective neutron counters were called N_1, N_2, N_3, N_4 . The anti-coincidence counters were placed so as to form four sides of a box around the target; they subtended approximately 70% of the solid angle available to decay electrons from stopping muons. On the side facing the target each counter was covered only with 0.00075 in. of aluminum foil and 0.001-in. black Mylar. These precautions were taken lest muons stop in low atomic number materials and be captured there. The A counters were used in four ways in the experimental logic (see Fig. 6): (1) as a prompt anticoincidence at muon arrival time to warn of a muon having left the target and having penetrated the scintillator; (2) in coincidence with the neutron detectors to define electrons; (3) in prompt anticoincidence with a pulse in the neutron detector to exclude electrons from consideration as events; and (4) as a 10- μ -sec anticoincidence (on film) to reduce accidental background.

The neutron detectors consisted of 1.8 liters of liquid scintillator NE213 which was purified, deoxygenated, and sealed in specially constructed glass vessels 6 in. \times 5 in. \times 4 in. An EMI 9530B photomultiplier directly viewed a 5- \times 6-in. face of the rectangular volume. Magnesium oxide was used as a reflective packing.

The largest single source of counts in the neutron

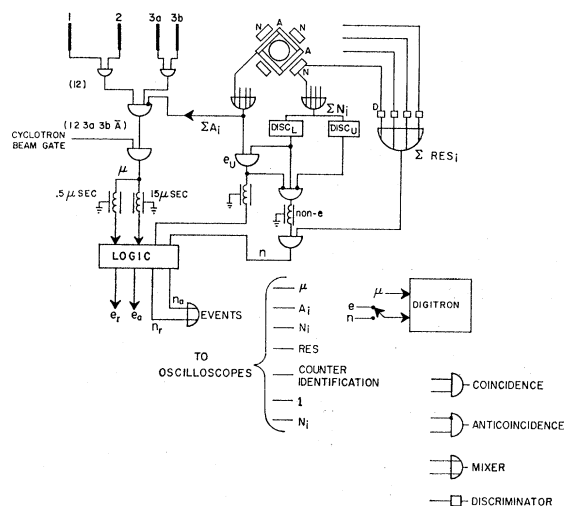


FIG. 6. Simplified block diagram of electronic logic used in muon capture experiment. The block marked “logic” refers to the muon triggered slow gating system used to gate “real” and “accidental” neutrons and electrons.

counters was gamma rays due to bremsstrahlung of the muon decay electrons in their passage through the high- Z target walls. In order to distinguish between neutron and gamma-ray induced recoils in the detector, pulse shape analysis of the form developed by Brooks¹⁵ was employed. The light produced by a charged particle in a scintillator is composed of a long-lived (~ 300 nsec) component superposed on a 10-nsec initial pulse. The size of the slower component is always proportional to energy loss, while the fast pulse is linear only for minimum ionizing particles and saturates for particles with a high rate of energy loss dE/dx such as 1–5-MeV protons. Thus, one can distinguish proton recoils from electrons by the ratio of the two components of the light pulse.

The same properties of the scintillation material which enable neutron-gamma ray discrimination are responsible for a nonlinearity in the energy response to proton recoils. This nonlinearity was measured in an independent experiment using the Nevis neutron velocity selector as a source of neutrons of known energy.¹⁶ Figure 7 shows the pulse-height response to protons

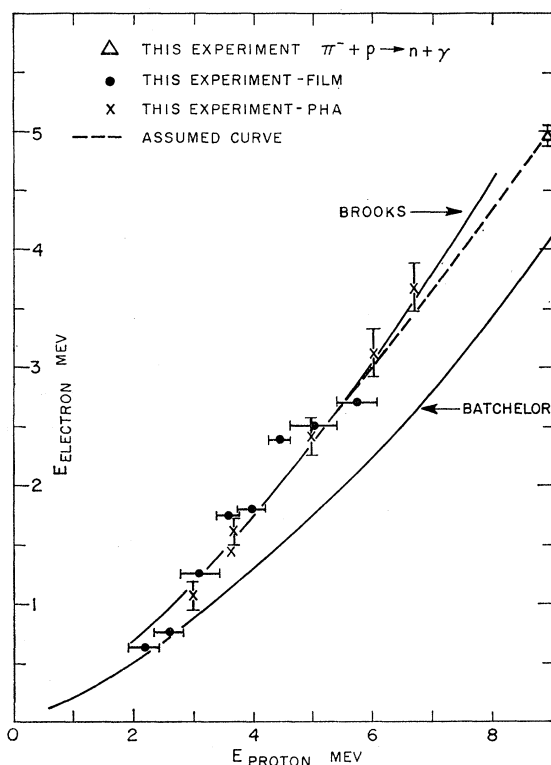


FIG. 7. The pulse-height response of scintillator NE 213 to protons. Experimental points were obtained using the Nevis neutron velocity selector, and one point was obtained from pion capture measurements. The solid curves are those of Brooks and Batchelor. The dashed curve was the one used in the analysis.

¹⁵ F. D. Brooks, *Progr. in Nucl. Phys.* **5**, 252 (1956); F. D. Brooks, *Nucl. Instr. Methods* **4**, 151 (1959); J. B. Birks, *Phys. Rev.* **94**, 364 (1951); R. Batchelor, W. B. Gilboy, J. B. Parker, and J. H. Towle, *Nucl. Instruments and Methods* **13**, 70 (1961).

¹⁶ This measurement is described in the Appendix. For further details see J. E. Rothberg, Nevis Report No. 116 (1963).

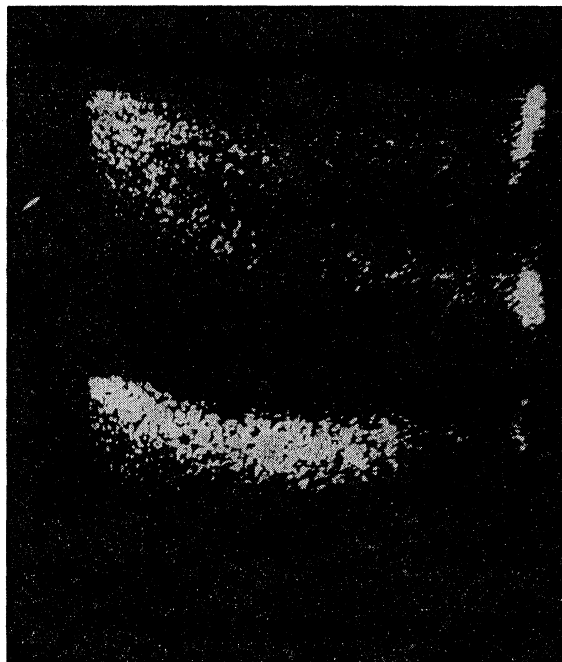


FIG. 8. Photograph of oscilloscope display of neutron and gamma-ray pulse height versus slow component residue. Horizontal axis is energy, increasing toward the right. The neutron residue is displayed on the vertical axis increasing downward. Upper photograph shows gamma ray and neutron "bands" due to a Pu-Be source. Lower picture is "band" due to a pure gamma-ray source (Cs^{137} —0.67 MeV).

compared with pulse-height response to Compton electrons. Knowledge of the distortion of the proton recoil spectrum due to the nonlinearity is vital if the spectrum is observed with a nonzero energy threshold and if the absolute number of detected neutrons is to be determined (see Appendix).

A circuit was designed which derived from the scintillator pulse shape a new pulse whose amplitude was a measure of the excess slow component, i.e., excess relative to the case of an electron pulse. This pulse along with the fast component pulse was recorded for each event. During the experiment the performance of the counters was monitored. In this monitor system, the slow component excess pulse and the fast pulse were stretched and applied to the x and y deflection plates of an oscilloscope. By unblanking the oscilloscope beam at the proper time, a spot was formed whose position signified whether a Compton electron from a γ ray or a proton recoil was detected (see Fig. 8). The response of the neutron detectors was periodically checked with a series of gamma-ray sources whose energy was in the region of interest: Cs^{137} —0.67 MeV, Co^{60} —1.25 MeV (the detectors are not able to resolve the two closely spaced lines) Na^{24} —1.38 MeV and 2.76 MeV. The neutron-gamma ray discrimination quality was checked every few hours using a plutonium-beryllium source which emits neutrons of energy up to about 6 MeV and gamma rays of 4.4 MeV.

E. Data Recording

A set of scalars with automatic printout was used to record the following information (see Fig. 6):

elapsed time, coincidence between first two beam counters = (12),

muon beam = (123a3b),

muons not leaving target = $(123a3b)(\Sigma A_i) = \mu$,

ungated decay electrons = $e_u = (\Sigma N_i)(\Sigma A_i)$,

neutral particles converting in the neutron detector = $(\Sigma N_i)\bar{e}_u$,

neutrons (slow component residue is sufficiently large) = n ,

muon gated electrons = e_r, e_a ,

muon gated neutrons = n_r, n_a .

The subscripts r, a , stand for "real" and "accidental"; n_r and n_a serve as oscilloscope triggers. The notation (ΣA_i) or (ΣN_i) refers to the mixture of the four detector outputs. In addition to the requirements noted above, each " μ " signal had to pass the "beam gate"; that is, it was used only if it occurred during the 8 msec when the meson beam was being ejected with good duty cycle. The requirement, $n\bar{1}$, discarding events which are in coincidence with an incoming pion, was omitted from the logic but was enforced when the oscilloscope photographs were analyzed.

To permit careful time and energy measurements as well as to check neutron-gamma ray discrimination and anticoincidence operation, several detector pulses displayed on the Tektronix oscilloscopes 517 and 555 were photographed. A mirror system permitted the use of a single camera. Both the oscilloscopes and the film advance mechanism were triggered on the arrival of either an n_r or n_a signal; that is, a muon gated neutron that occurred during a 5 μ sec interval beginning either $\frac{1}{2}$ μ sec after a muon pulse of 15 μ sec thereafter. The fast pulse and the slow residue pulse from the neutron detector, the pulse from beam counter No. 1, a muon pulse, the pulse from the A counters, and a neutron counter number identification were recorded on film.

Simultaneously with data being taken on film, a "digitron" system received pulses representing the muon and electron, and stored the time interval distribution in a 400-channel RIDL pulse-height analyzer, making possible lifetime measurements of very high statistical accuracy.¹¹

For each individual neutron detector, for the data accumulated during each day of running, a plot was made of the size of the fast pulse in the neutron detector against the size of the slow residue. This plot is analogous to the type of oscilloscope display that was available during the run. An example is given in Fig. 9. With these plots all events which fell in the region of gamma rays could be eliminated and for each detector the lowest energy that would permit reliable neutron-gamma ray discrimination could be determined.

Muon-neutron time distributions were plotted from these events. These are shown for the two geometries in

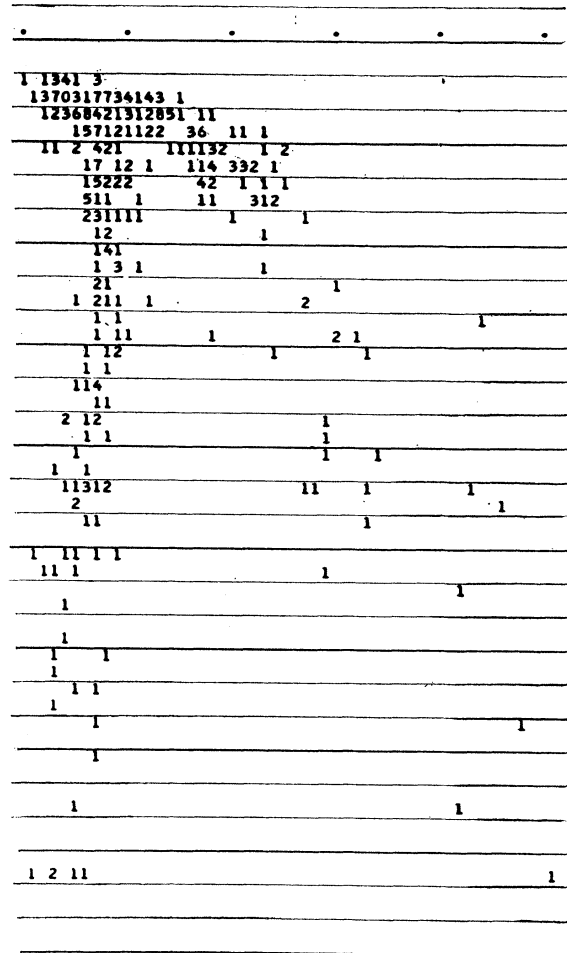


Fig. 9. Plots of pulse height versus residue for neutron and gamma ray radioactive sources. Increasing energy is downward; neutron residue increases toward the right. The plots were generated from data taken from measurements of oscilloscope traces photographed during the experimental run. The numbers in the plot refer to the number of events in each "bin."

Fig. 10. They are characterized by an approximately 2.2- μ sec lifetime component, as is expected from muon capture in hydrogen, and a 0.2- μ sec component from captures in iron.

III. ANALYSIS

A. Calculation of Capture Rate

The experimental value of the muon capture rate is given by

$$\text{Rate} = \frac{N_n - N_B}{E\Omega_n T} \frac{1}{N_\mu} \lambda_0,$$

where N_n is number of detected neutrons, N_B represents neutrons due to sources other than hydrogen capture, E is detector efficiency, Ω_n is the detector solid angle, and N_μ is the number of muons stopping in hydrogen. T is the time gating factor.

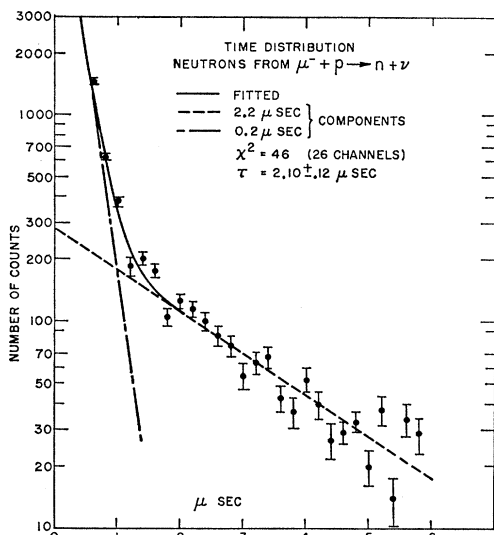


FIG. 10. Time distribution of neutrons from $\mu^- + p \rightarrow n + \nu$. Time interval measurements were obtained from scanning of film; accidental events have been subtracted but iron capture neutrons are in evidence at early times. The best fit for the lifetime is 2.10 ± 0.12 μ sec. A similar set of data taken with the 3-in. geometry shows a lifetime of 2.13 ± 0.15 μ sec.

1. Muons Stopping in Hydrogen

One can arrive at the number of muons stopping in hydrogen in two ways; from the number of $(123a3b)\bar{A}$ counts, or the number of $(e_r - e_a)$ decay electrons. Several corrections must be made to the raw number of beam counts to obtain a muon stopping number. These are due to muons stopping in the front wall of the target etc. Experimental runs with a simulated target were carried out in order to measure the muon stopping distribution and to determine the percentage of " μ " counts which are muons entering the target region. It was found that only about three-fourths of the $(123a3b)\bar{A}$ triggers represent muons which leave the last collimator, the rest having trajectories which failed to enter the target.

The second method of determining the muon stopping number is more reliable. The important advantages are: (i) Except for a small and known number of accidentals, a $(\mu)e$ delayed coincidence can only be a decay electron; (ii) electrons are required to pass the same time gate as neutrons; (iii) electrons are detected with the same neutron detectors (and hence almost the same solid angle) as are neutrons; (iv) since the time gate is sufficiently delayed, only decay electrons from muons stopping in hydrogen are counted. The number of muons stopping in hydrogen is given by

$$N_\mu = (e_r - e_a) / T \Omega_e L,$$

where T is the time gate factor, Ω_e is the solid angle for electron detection, and L is a loss factor for electrons due to target side walls.

In Table I the determination of the muon stopping number (N_μ) is outlined; $(e_r - e_a)$ has been set equal to

TABLE I. Determination of muon stoppings.

Geometry	$e(10^6)$	T	Ω_e	L	$N_\mu(10^6)$
3 in.	8.62	0.774	0.185	0.9	67.0
4 in.	11.40	0.732	0.185	0.9	93.6
Uncertainty	~ 0	$\pm 1.0\%$	$\pm 1.8\%$	$\pm 5.0\%$	$\pm 5.5\%$

e . In the negative beam e_a/e_r is 1.5% and 2.1%, respectively, for the 3- and 4-in. geometries. The time factor was deduced from the lifetime plot (Fig. 10) assuming a decay lifetime of 2.2 μ sec, noting that the same muon-generated univibrator output gates both electrons and neutrons. The solid angle for detection of an electron assuming the known muon stopping distribution in hydrogen was calculated, using the same Monte Carlo code as was used for the neutron detector efficiency calculation. A small correction was applied to account for edge effects in the neutron detector.

The electron loss factor, L , consists of several effects of which the largest and most difficult to calculate was radiation in the high Z target walls. This effect (5%) was directly measured with the dummy target and simulated target walls. Another 5% of the electrons were lost due to counter walls and energy threshold. Thus, a loss factor of $(10 \pm 5)\%$ is used to correct the observed number of electrons.

2. Time Gate Factor

From the neutron time distribution plot a time interval was chosen which excluded most of the iron capture events; only the data within this new time interval was analyzed to extract the muon capture rate. Events occurring at earlier times were isolated and used to provide an energy spectrum of neutrons from muon capture in iron.

3. Solid Angle and Detector Efficiency

The total solid angle subtended by the four neutron detectors was calculated to be 19.6% given the measured muon stopping distribution.

A complete calculation of neutron detector efficiency was carried out. This Monte Carlo code included the following complications: (i) the neutron detectors were surrounded by lead and other materials which might "reflect" neutrons; (ii) the path length in the detector is direction-dependent; (iii) neutron cross sections are energy-dependent; (iv) the detectors are thick enough to permit multiple recoils; (v) scattering and energy loss in the hydrogen target; (vi) the response of the detectors is nonlinear (see Fig. 7) for protons of the relevant energies (< 5.2 MeV); (vii) the detector contains carbon as well as hydrogen.

The calculation gives the final expected yield as a function of detector energy threshold. Although it is not completely meaningful to decouple the several effects, since the electron yield depends on the solid angle also (which essentially "cancels out" in the final capture rate), it is interesting to list the extent to which

each effect determines the final neutron yield. The numbers are approximate and are not needed in the analysis.

Fraction of neutrons observed due to effect of:

Solid angle	0.20
Hydrogen target degradation	0.90
Detector mean free path	0.50
Energy threshold (1 MeV)	0.36

Figure 11 shows the corrected neutron pulse-height distributions together with the calculated pulse-height spectrum for each of the detectors and each geometrical arrangement.

4. Corrected Number of Detected Neutrons

Several corrections were applied to the number of neutron events.

(i) *Accidentals.* Random background events were accumulated by triggering on neutrons occurring during a gate which was delayed 15 μ sec. For the 3- and 4-in. geometries the accidental events rate was 0.39 and 0.49 counts per μ sec per million muon stoppings, respectively. The accidental rate in the real gating interval was reduced by the requirement that no anti-coincidence counter pulse (*A* pulse) appear on the trace. The effect of this requirement was measured by considering the time distribution of *A* pulses relative to neutron pulses and also with respect to muon pulses. The fraction of the *A* pulses which were correlated in time with neutron pulses represent $N\bar{A}$ failures. Those that appear after a muon but are uncorrelated with a neutron represent muon decays which are detected with the large solid angle of the *A* counters. Exclusion of these events results in decreased accidental background. The number of random *A* pulses was determined by scanning for pulses which preceded the muon stopping. The normalized energy spectrum of accidentals was subtracted from that of the real neutron events.

(ii) *Neutron events in the positive beam.* In order to evaluate possible spurious events due to the high flux of decay electrons entering the neutron detectors, it was desirable to count decay electrons in the absence of muon capture neutrons. This situation is realized by stopping positive muons in the hydrogen target. It was found that a nonnegligible rate of neutron events persisted under positive beam running conditions. These events were found to have the time distribution of decay electrons and are explained as being due to photonuclear processes produced by the electron bremsstrahlung. The effect has been considered and the observed neutron rate was found to be consistent with that expected on the basis of $C^{12}(\gamma, p)$ and $C^{12}(\gamma, n)$ reactions occurring in the neutron detectors.

That the positive beam neutron events are electron associated is confirmed by the 2.2- μ sec exponential time distribution of these events. The possibility of stopping positive muons in the hydrogen, where the physical situation is identical except for the absence of capture neutrons, allows an accurate correction to the data independent of knowledge of the source of events.

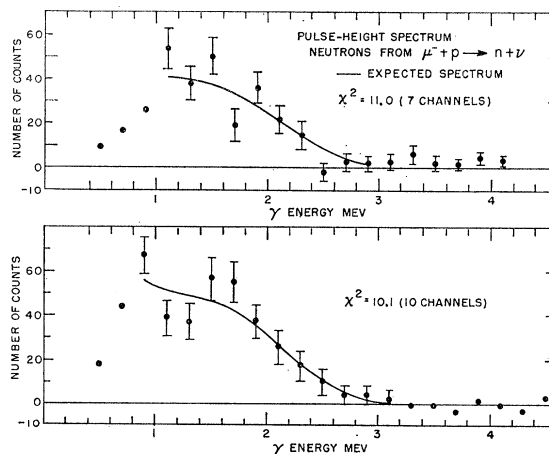


FIG. 11. Pulse-height distribution of corrected neutron events from $\mu^- + p \rightarrow n + \nu$. Each neutron detector and each geometrical arrangement was plotted individually. The horizontal scale is in MeV as calibrated with gamma-ray sources. The data in Fig. 7 is used to convert to neutron energy. The results of a Monte Carlo calculation of detector response are shown as a solid curve. It was fitted by normalization. The upper curve is data taken with detector N_1 in 4-in. geometry; the lower one is N_2 in 3-in. geometry. The χ^2 values of the fit are 11.0 (7 channels) and 10.1 (10 channels), respectively.

(iii) *Wall capture events.* The neutron time distribution reveals a contribution from muon capture in iron. It will be shown later that there is no reason to expect a substantial contribution from any material other than iron. The energy spectrum of neutrons from muon capture in iron was determined in two ways. In a preliminary measurement a study was made of the neutron yields and spectra from muon capture in various materials, including carbon, iron, silver, zirconium, and lead. An additional determination of the iron spectrum was obtained by considering only the early time segment of the actual data (see Fig. 10) and subtracting from this the appropriate number of accidentals and of events with 2.2- μ sec lifetime.

The neutron yield from iron was normalized to the number obtained from the time distribution and the gating interval location and was subtracted from the neutron events spectrum. The gating interval was chosen so as to keep the subtraction small.

(iv) *Scanning and statistical corrections.* The maximum film advance rate in the oscilloscope photography system was one frame per second. The number of neutron events was corrected for the number of events lost because of confusing overlap of pulses on the trace and because of superimposed traces. The total correction was $13.0\% \pm 0.6\%$, and $21.3\% \pm 0.6\%$ for the 3-in. and 4-in. cases, respectively. This correction contributes only a negligible error to the final result by virtue of a complete tabulation and record of lost events. There was no scanning efficiency correction since each film frame was accounted for on an IBM card, and event rejection took place during analysis of the cards.

The neutron pulse-height spectrum was plotted for each detector in each geometrical arrangement. De-

TABLE II. Calculation of capture rate.

Counter	4-in. geometry			3-in. geometry		
	N_1	N_2	N_4	N_1	N_2	N_4
Energy interval (MeV)	0.8 to 2.8	1.0 to 2.8	1.4 to 2.8	1.2 to 2.8	1.0 to 2.8	1.2 to 2.8
Neutrons	547.0±26.2	441.5±23.1	264.4±17.7	288.2±18.1	340.1±19.5	227.2±16.3
Accidentals	39.0±6.9	17.1±4.6	9.0±3.3	39.6±6.7	19.2±4.6	11.5±3.4
Positive beam events	116.1±13.5	140.7±15.0	65.1±10.0	62.0±8.6	48.8±7.6	29.0±5.9
Iron captures	14.8±4.2	9.9±3.5	5.7±2.6	8.0±3.0	8.1±3.0	5.8±2.4
Corrected events	377.1±30.4	273.9±28.1	184.6±20.9	178.6±21.5	264.0±21.8	180.9±17.9
Percentage error	8.05%	10.3%	11.4%	12.0%	8.3%	9.9%
	rms error	4.1%				
(eff) ^a ×(10 ⁴)	320.9(±5.0%)	274.6	181.2	227.8	274.6	227.8
eff×Ω	75.5(±5.4%)	74.1	46.0	51.5	73.3	59.5
$N_{\mu}' \times (10^{-6})$	43.2(±5.6%)	43.2	43.2	32.6	32.6	32.6
(eff)(Ω)(N_{μ}')(10 ⁻³)	326.0	320.0	198.5	167.8	238.0	194.0
Rate ⁻¹ (N_{μ}'/n)	865	1171	1072	940	903	1071
Rate (sec ⁻¹)	527±59	388±50.4	425±59	485±70	505±57.5	425±54
	Wt. av		469±42			

^a In the above Table "eff" is detector efficiency; "Ω" is percentage solid angle for each detector determined from electrons; " N_{μ}' " is (N_{μ}) × (gate factor). The six values for the capture rate considered as a distribution about their mean have a χ^2 of 7.4. The final error of the mean includes contributions from the six independent errors as well as the errors in muon stopping rate and in detector efficiency which are the same for all six cases. The average capture rates in the 4-in. and 3-in. situations are 464.0 and 475.0, respectively.

tector N_3 was eliminated from detailed consideration since the quality of neutron-gamma ray discrimination was doubtful for a large fraction of the data. The calculated detector response was fitted to each energy spectrum by equalizing the areas above some chosen energy (on the gamma-ray energy scale); no scale change or other adjustment was needed beyond the original conversion of arbitrary pulse height units to energy (MeV) using radioactive source data. Figure 11 shows sample plots along with the χ^2 calculated after the expected curve was fitted.

The data were grouped into two energy blocks, one beginning at a low energy depending on the detector and ending at 2.8 MeV (corresponds to 5.8-MeV proton recoils) and the other entirely above the expected neutron energy from 3.2 to 4.2 MeV (gamma scale). The data in the first block were used to obtain the capture rate as in Table II, while the second block in Table III demonstrates the cancellation of events above the expected energy providing additional confirmation that background has been subtracted properly. Muon capture in materials other than hydrogen has been observed to yield neutrons whose energy spectrum extends above 5.2 MeV. Thus an additional confirmation of the hydrogen purity is obtained.

5. Small Corrections to the Capture Rate

(a) *The presence of deuterium in the hydrogen.* The fraction of muons transferred to the deuterium branch of the diagram in Fig. 1 is

$$F = c\lambda_e / (\lambda_{pp} + \lambda_0 + c\lambda_e);$$

the concentration of deuterium in the target was less than one part per million. Using the measured values for the constants

$$\begin{aligned} \lambda_0 &= 0.455 \times 10^6 \text{ sec}^{-1}, \\ \lambda_{pp} &= 1.9 \times 10^6 \text{ sec}^{-1}, \\ \lambda_e &= 1.4 \times 10^{10} \text{ sec}^{-1}, \end{aligned}$$

we obtain

$$F = 0.007.$$

Actually, not all the muons which transfer to deuterium fail to give a measured neutron. In any case the effect of deuterium is negligible.

(b) *Other impurities in the hydrogen.* Assume a transfer rate to higher atomic number impurities $\sim 5 \times 10^{10} \text{ sec}^{-1}$; the concentration of these impurities is $\sim 10^{-12}$, certainly less than 10^{-9} . In the latter case $F = 2.5 \times 10^{-6}$. Even though the capture rate is higher than that in hydrogen by ~ 200 , the fraction of neutrons from capture in these impurities is 0.005 at most, again negligible.

Note added in proof. The direct experimental checks of this statement are twofold. (i) The 4-in. geometry run and the 3-in. geometry run were consecutive and each lasted about eight calendar days. The results of each run (Table II and footnote) with statistical error only are: 464 ± 13 and $475 \pm 16 \text{ sec}^{-1}$. The invariance to time places a limit of 6 percent on the contribution of any possible leak or outgassing induced impurity. (ii) The absence of neutrons above 5.2 MeV (Table III), using observed neutron spectra from carbon places a limit $\lesssim 1$ percent on the contribution of low Z captives (from H_2 impurity or counter stoppings) to the final result.

TABLE III. Calculation of rate of events above muon capture neutron energy. Energy interval=3.2-4.2 MeV (gamma-ray scale).

Neutron counter	4-in. geometry			3-in. geometry		
	N_1	N_2	N_4	N_1	N_2	N_4
Neutrons	17.0±4.6	12.1	17.0	18.1	15.9	13.6
Accidentals	2.9±1.7	1.2	2.2	2.8	0.9	0.0
Positive beam events	23.8±6.0	5.9	18.5	14.6	8.2	14.8
Iron captures	1.0	0.6	0.8	1.0	0.7	1.0
Corrected events	-10.7±7.8	4.4	-4.5	-0.3	6.1	-2.2
Average	-1.2±3.0					

(c) *Captures in carbon (outside the target).* There are only three possible sources of carbon capture; great efforts having been made in the construction of the target to eliminate all low- Z material. Plastic scintillator was the only remaining potentially dangerous material.

(i) Muons stopping in counter No. 3a: The accidental rate of the (123a)3b coincidence was 10/min. These accidentals might represent stoppings in the No. 3a counter. Including the ratio of solid angles of this detector to the hydrogen (0.06) and the ratio of capture rates (100), the fractional yield due to this mechanism is ≤ 0.0025 . This is completely negligible

(ii) Muons stopping in counter No. 3b: The differential stopping distribution curve for muons indicates that in the vicinity of counter No. 3b the stopping rate is 500/g while in the peak of the distribution the rate is 3000/g. The counter is 0.05 g thick so that the ratio of muons stopping in the counter to those stopping in hydrogen is 0.002. The ratio of solid angles is 0.07, the extra length of hydrogen causes further attenuation of the neutron yield by about a factor of 2. The percentage neutron yield from this source is 0.7%.

(iii) Muons penetrating the anticoincidence detectors: This case was an important one to investigate carefully since the solid angle for detection of any neutrons produced in the anticoincidence detectors was larger than that for hydrogen neutrons. It was possible to obtain a sufficiently accurate estimate of this source of background by considering the number of muons stopping in the target walls. The latter number can be obtained in several ways. The iron in the target wall comprises 0.495 g while the higher Z components together comprise 2.69 g (with an average Z of 42).

Analysis of the neutron data taken on film gives the following result for the ratio of muons stopping in iron to those stopping in hydrogen: 4-in. geometry—(0.78±0.11)% and 3-in. geometry—(0.55±0.08)%. The neutron time distributions as recorded on the digitron clearly show both a high- Z component and an iron component in the lifetime. From this data one can obtain, independently of solid angle and efficiency, the ratio of muon stoppings in high Z to the stoppings in iron: 4-in. geometry—3.6±0.4, and 3-in. geometry—6.1±0.6, while the ratio of densities is 5.45. One then has for the percentage of muons stopping in the higher Z component of the walls:

$$4\text{-in.}-(2.8\pm 0.7)\%, \quad 3\text{-in.}-(3.4\pm 0.8)\%.$$

An independent estimate of the number of muons stopping in high- Z materials comes from a comparison of the yield of decay electrons per muon in the positive and negative beams. From this source one obtains: 4-in.—(5.5±2.2)% 3-in.—(3.5±1.4)%. This is in rough agreement with the previous estimate.

Thus the wall stopping rate for muons in the vicinity of the target walls is 1.4% of the muons per gram of wall material. Since muons were at the end of their range

having penetrated much hydrogen, etc., the rate of stopping was surely decreasing with increasing thickness and, therefore, is expected to be somewhat lower than 1.4% at the position of the anticoincidence detector. Nevertheless, this number was used to obtain an upper limit. A further check on the above estimate is the observation that the electronic requirement (123a3b) \bar{A} reduces the counted number of muons by (1±0.3)% below the (123a3b) rate. Since the anticoincidence detector is 1 g thick the estimate of muons penetrating it is confirmed.

Analysis of film taken of decay electron events shows that one can easily measure pulses whose size is one-fifth of the size of the pulse due to a minimum ionizing particle passing through the detector. For the anticoincidence detectors of the thickness used, one-fifth minimum ionizing corresponds to an energy loss of 0.5 MeV. A stopping muon which leaves 0.5 MeV in the plastic comes to rest after 0.0035 g. The Mylar and aluminum coating on the counters are 0.007 g thick. Assuming a total low- Z thickness of 0.011 g wherein a stopping muon would go undetected, one has as a ratio of carbon stopping muons to muons stopping in hydrogen, 1.5×10^{-4} . Including a solid angle enhancement factor and a capture rate factor, we have as an upper limit on the neutron yield ratio 1.8%. A more realistic estimate is probably 1%. Although it is much smaller than the quoted error, a correction factor of (−1±0.5)% is included. See also paragraph 5(b) above.

(d) *The admixture of (μp) atomic capture in the data.* The (μp) atomic system converts to the ($p\mu p$) molecular ion with a rate $\lambda_{pp} = 1.9 \times 10^6 \text{ sec}^{-1}$ or a partial lifetime of about 0.5 μsec . The data that were used in the analysis were taken in a time interval beginning at 1.2 μsec so that the admixture of (μp) is quite small. Nevertheless, it is easy to calculate the exact effect on the capture rate. Using the usual coupling constants, the capture rate in the molecular state is expected to be 560 sec^{-1} while the singlet atomic capture rate is about 640 sec^{-1} . The rate for a mixture of the two which is observed from $t=t_0$ to infinity is

$$R = \lambda_{(p\mu p)} + \frac{\lambda_0}{\lambda_0 + \lambda_{pp}} (\lambda_{(\mu p)} - \lambda_{(p\mu p)}) e^{-(\lambda_{pp})t_0}.$$

In the present experiment the effect is very small but in a bubble chamber experiment ($t_0=0$) the rate is expected to be enhanced by about 4%.

(e) *Possible molecular ortho-para conversion.* The rate of transition of the ortho state to the para is expected to be quite negligible on the scale of muon lifetimes.^{2,9} One can obtain an upper limit to the decay rate from the neutron-muon time interval distribution curves (Fig. 10) by noting that the capture rate in the para state is expected to be about 220 sec^{-1} as opposed to 560 sec^{-1} in the ortho molecular state. The experimental upper limit to the ortho-para conversion rate λ_{op} is then $0.05 \times 10^6 \text{ sec}^{-1}$ corresponding to a partial lifetime of 20 μsec . In the unlikely circumstance that this were

in fact the conversion rate, the expected capture rate would be reduced to about 525 sec^{-1} .

6. Summary

The final estimate for the capture rate is $464 \pm 42 \text{ sec}^{-1}$. A small correction has been applied for the effects mentioned in the last section. It can be seen from Table II that the error is principally due to three sources: (a) the various subtractions to the spectrum, (b) the number of muons stopping in the hydrogen, and (c) the detector efficiency calculation. The statistical error in the raw number of detected neutrons is rather small, but the above three categories contribute roughly 4%, 5%, and 5%, respectively.

IV. PION CAPTURE: A CONFIRMING MEASUREMENT

A. Introduction

It was desirable to apply the target, detector geometry, and efficiency calculation to a similar experiment which was somewhat easier to carry out and whose result was predictable. A natural choice for the check experiment was pion capture. When a negative pion comes to rest in hydrogen, it always interacts with a proton. Recent measurements¹⁷ show that the time interval between a pion velocity of $0.006c$ and nuclear interaction is about $2.3 \times 10^{-12} \text{ sec}$ in liquid hydrogen. The interaction modes that occur are

- (a) $\pi^- + p \rightarrow \pi^0 + n$ (0.41 MeV),
- (b) $\pi^- + p \rightarrow \gamma + n$ (8.9 MeV).

The Panofsky ratio which has been measured many times is defined as the ratio of probabilities $a/b = P$. The quantity measured in this experiment is $R = 1/(1+P) = b/(a+b) = 0.396$, using the most recent value for P .¹⁸

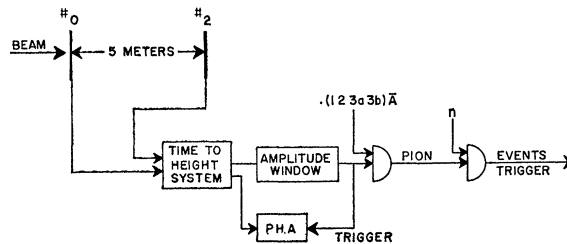
B. Description of Experiment

The pion capture experiment can be performed with no change in the experimental arrangement other than that needed to stop a known number of pions in the target. This was accomplished by reverting to the normal unpurified meson beam situation and installing the time-of-flight system. The output of the time-to-height converter was sent to a pulse-height window which selected pions in the beam; the signal from the window output was then put in coincidence with the usual "muon stopping" pulse, providing a trigger which was free of muons and, more important, of electrons. Since pion capture is a prompt process, the muon triggered delayed gate was shortened in length and its delay was decreased so as to be in prompt coincidence with the pion stopping pulse (Fig. 12). Because of the relatively high "events" rate it was possible to take data on a pulse height analyzer as well as on film.

Neutron-gamma ray discrimination was checked

¹⁷ J. H. Doede, R. Hildebrand, M. H. Israel, and M. R. Pyka, Phys. Rev. **129**, 2808 (1963).

¹⁸ J. Ryan, Phys. Rev. **130**, 1554 (1963).



PION CAPTURE LOGIC

FIG. 12. A simplified block diagram of the part of the electronic logic peculiar to the pion capture experiment (see Fig. 6 for notation and rest of logic). The pulse-height analyzer (PHA) shown was used to monitor pion beam purity. A second PHA was gated on "events" and displayed the neutron pulse-height spectrum.

using the pion capture neutrons and gamma rays themselves, in addition to the radioactive sources. Energy calibration was possible using the 4.4-MeV carbon gamma ray from a plutonium-beryllium source ($\alpha + \text{Be}^9 \rightarrow n + \text{C}^{12*}$, $\text{C}^{12*} \rightarrow \text{C}^{12} + \gamma$) and the Na^{24} source for the lower end of the scale. A high-energy point was fixed using the 6.14-MeV gamma ray from the following reaction: $n + \text{O}^{16} \rightarrow \text{N}^{16} + p$, $\text{N}^{16} \rightarrow e^- + \text{O}^{16*} + \bar{\nu}$, $\text{O}^{16*} \rightarrow \text{O}^{16} + \gamma$ (6.14 MeV).

There is such an abundance of pion capture neutrons that even if the detector energy response were unknown it would be self-determining at the 8.9-MeV point. The high-energy point obtained in this way helps to confirm the earlier independent measurement of the scintillator energy response.

C. Data and Results

To calculate the fraction of pions captured in the one observable mode, it was necessary to obtain the actual number of pions stopping in hydrogen. Since the $(123a3b)$ signal was gated on pions alone (time-of-flight criterion) it was sufficient to apply the same factor (the ratio of muons stopping in hydrogen to beam counts) as was used in the muon experiment.

Only one correction to the neutron spectrum data was needed; it is expected that the same number of pions stop in wall materials as did muons in the principal experiment. However, wall captures here are coincident in time with pion arrival, as also are the captures in hydrogen. Thus wall captures play a relatively larger role in pion capture where the device of delayed counting is not effective. A crude estimate of the number of neutrons expected from wall interactions was made and agrees with the actual correction which was performed in a self-determining manner. In the neutron energy spectrum plot a flat low level of counts persisted beyond the clearly visible cutoff energy of hydrogen events. The low background level was extrapolated back toward zero with the appropriate rise. The total subtraction in the energy region of interest amounted to $12.8 \pm 3\%$. The neutron energy distribution obtained from analysis of the film was plotted and fitted (by

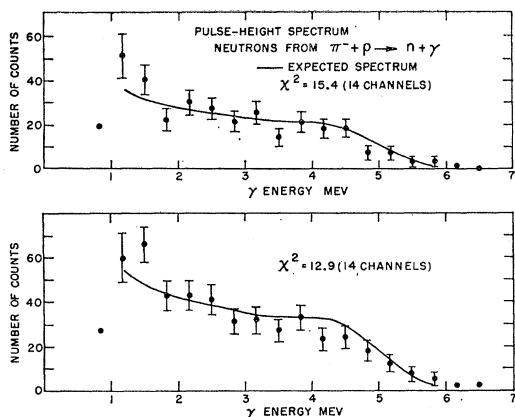


FIG. 13. Pulse-height distribution of neutron events from the reaction $\pi^- + p \rightarrow n + \gamma$. Two independent runs are shown, each fitted with the results of a Monte Carlo calculation of detector response. Energy scale is in MeV as calibrated with γ -ray sources.

normalization only) with the calculated detector response curve (Fig. 13). Only a change in one parameter (the initial neutron energy) was needed to convert the Monte Carlo code for detector response from the muon capture to the pion capture situation. Table IV lists

TABLE IV. Calculation of pion capture branching fraction.

Run	De- tected neu- trons	Corrected neutrons	Pion stops (10^6)	Actual neutrons (10^6)	Branching fraction R
<i>a</i>	720	628 ± 40	(0.192 ± 0.011)	77.8 ± 6.4	0.405
<i>b</i>	1468	1280 ± 69	0.387	159.0 ± 11.7	0.411
<i>c</i>	685	597 ± 43	0.185	74.1 ± 6.6	0.401
				Average	0.407 ± 0.035
				Expected	0.396

the data and results of three independent runs of the pion capture experiment.

The agreement between the measured value of the branching fraction and the one expected on the basis of more precise experiments indicates that in the muon capture experiment, the muon stopping number, wall effect and the detector efficiency were assessed correctly.

V. RESULTS AND CONCLUSION

The present muon capture experiment yields a single experimentally determined number; the capture rate in the $(p\mu p)$ molecule. The presence of iron capture neutrons appearing at early times made it impossible to extract a meaningful value for the (μp) atomic capture rate (singlet). The corrected experimental result for the molecular capture rate is given in Table V, together with other existing results.^{5,19,20}

¹⁹ R. H. Hildebrand, and J. H. Doede, *Proceedings of the 1962 Annual International Conference on High Energy Physics at Geneva* (CERN Scientific Information Service, Geneva, Switzerland, 1962), p. 418.

²⁰ E. Bertolini, A. Citron, G. Gianianella, S. Focardi, A. Mukhin, C. Rubbia, and S. Saporetti, *Proceedings of the 1962 Annual International Conference on High Energy Physics at Geneva* (CERN Scientific Information Service, Geneva, Switzerland, 1962), p. 421.

TABLE V. Muon capture results.

Experiment	Result (sec^{-1})	Expected (sec^{-1})
Columbia ^a	515 ± 85	562
Chicago ^b	435 ± 100	580
CERN ^c	420 ± 75	580
This experiment	464 ± 42	562

^a See Ref. 5. ^b See Ref. 19. ^c See Ref. 20.

There are several possible interpretations of a discrepancy between the observed and predicted rates.

(i) The present calculated value of the molecular wave-function overlap could be in error by $\sim 10\%$.

(ii) The equality of the electron and muon axial vector coupling constants is implied by the observation of the ratio of the reactions $\pi \rightarrow e + \nu$ and $\pi \rightarrow \mu + \nu$. At the momentum transfer of muon capture, the axial vector coupling constant is modified by a term of order (m_μ^2/M_p^2) which has a negligible effect on g_A . Anomalous behavior of the momentum dependence is considered unlikely.

(iii) It is possible that time reversal invariance fails in muon capture. If this is the case, then the vector and axial vector coupling constants could have a relative phase factor and the capture rate in the singlet state is reduced below what would be expected if $g_V = -g_A$. In the vicinity of 180° the phase factor is quite insensitive to the measured capture rate since the rate is at maximum there.

(iv) The conserved vector current theory identifies the momentum dependence of the vector coupling constant with that of the nucleon form factor. This identification allows the coupling constant g_V^μ to be evaluated at the muon capture momentum transfer. Effects of the conserved vector current have recently been clearly observed in the beta decay of the $B^{12} - N^{12}$ multiplet.²¹ Experiments on the decay $\pi^+ \rightarrow \pi^0 + e^+ + \nu$ are in progress and some have already measured a rate in rough agreement with the prediction of the conserved vector current theory.²² In view of the success of this hypothesis it is unlikely that either the vector coupling constant or the so-called weak magnetism terms differ from the predicted values.

(v) The success of the conserved vector current theory allows the value of g_V^μ to be obtained from the measured value²³ of g_V^β if suitable correction is made for differences in momentum transfer. In beta decay the ratio of g_A^β to g_V^β (-1.21) is obtained from comparison of the free neutron decay reaction with O^{14} decay which is a purely "vector" process. The present experiment can be interpreted as providing a direct measurement of g_A/g_V in the muon-proton interaction. The usual assign-

²¹ C. S. Wu, Y. K. Lee, and L. Mo, *Phys. Rev. Letters* **10**, 253 (1963).

²² P. Depommier, J. Heintze, A. Mukhin, C. Rubbia, V. Soergel, and K. Winter, *Phys. Letters* **2**, 23 (1962).

²³ R. K. Bardin, C. A. Barnes, W. A. Fowler, and P. A. Seeger, *Phys. Rev.* **127**, 583 (1962).

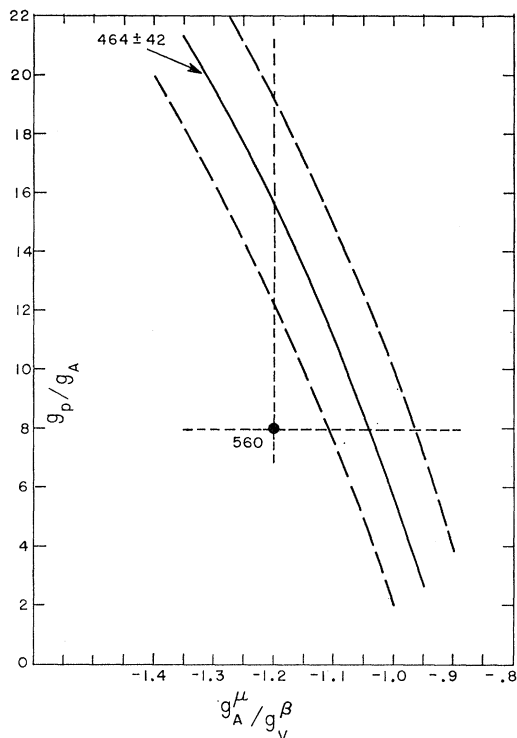


FIG. 14. Muon capture rates in the $(p\mu p)$ molecular ion with the axial vector coupling constant and the induced pseudoscalar coupling constant as independent variables. The point marked with a capture rate of 560 sec^{-1} corresponds to the usual choice of coupling constants. The band indicates the region consistent with the results of the present experiment.

ment of -1.21 to this ratio yields a molecular capture rate of 560 sec^{-1} . The results of the present experiment are consistent with a ratio $g_A/g_V = -1.05 \pm 0.08$.

(vi) The calculation²⁴ of the induced pseudoscalar coupling g_p could be in error. The usual result is $g_p/g_A = 8$ but there are several indications that this is in disagreement with observation. The large angular asymmetry of neutrons observed in the capture of polarized muons by spin zero nuclei is consistent with a larger g_p^μ/g_A^μ ratio.²⁵ The recent observation²⁶ of muon capture in O^{16} also yields a larger ratio than expected, but the interpretation depends on nuclear wave functions.

Using the expression for the muon capture rate with g_p/g_A and g_A/g_V as independent variables the molecular capture rate was computed. A band was plotted (see Fig. 14) in the plane of these variables that includes those points consistent with the results of the present

experiment. It can be seen that if the expected ratio of V to A is used, then a ratio of $g_p/g_A = 15.5 \pm 3.5$ is required in order to fit the data; whereas if $g_p/g_A = 8$ is assumed then g_A/g_V is required to be -1.05 ± 0.08 .

Note added in proof. Recent new bubble chamber results were presented at the Weak Interaction Conference, Brookhaven National Laboratories, Sept. 1963:

$$\text{CERN}^{20} \quad 450 \pm 50 \text{ sec}^{-1}$$

$$\text{Chicago}^{19} \quad 410 \pm 85 \text{ sec}^{-1}.$$

ACKNOWLEDGMENTS

We would like to acknowledge the important contributions of Dr. E. Zavattini of CERN who participated in our earlier work. We would like to thank W. LeCroy for the design of the time-of-flight system and for continual assistance in instrumentation. Dr. M. Kalos assisted in the design and planning of the Monte Carlo efficiency calculation; conversations with him were very helpful. S. Meravy assisted in the construction of the hydrogen target; he was responsible for its trouble-free operation during the experimental run. We thank Professor J. Rainwater for the use of the Nevis Neutron Velocity Selector facilities. The experiment could not have been carried out were it not for the dedicated and continual assistance of the entire Nevis Laboratory staff.

APPENDIX: PROTON RESPONSE IN NE 213

A. Introduction

When particles for which dE/dx is independent of energy, traverse a scintillating material the light output per centimeter, dS/dr , is constant. The generalization¹⁵ to nonrelativistic particles is

$$\frac{dS}{dr} = \frac{a(dE/dr)}{1 + b(dE/dr)},$$

with an extra "saturation" term in the denominator. The more heavily ionizing the particle the more severely quenched is the initial (~ 2 nsec) light output from the scintillating material. The slowly decaying component (~ 300 nsec) of light remains proportional to energy loss. Particle detection systems are sensitive primarily to the fast nonlinear component of light output. Therefore, the use of organic scintillators as energy spectrometers for protons requires that the nonlinearity of response of the scintillator be accurately known.

B. Description of Experiment

Experiments were carried out using the Nevis neutron velocity selector to determine the response of the organic liquid scintillator, NE 213, to neutron-induced proton recoils in the range 2 to 6 MeV. In this energy range, in a hydrogenous substance, ionization due to incident neutrons is entirely from elastic hydrogen collisions (at least at times short compared to thermalization time). The mean free path for 4-MeV neutrons in

²⁴ M. L. Goldberger and S. B. Treiman, Phys. Rev. **110**, 1178 (1958); **111**, 354 (1958); L. Wolfenstein, Nuovo Cimento **8**, 882 (1958).

²⁵ V. S. Evseev, V. S. Roganov, V. A. Chernogovova, M. M. Szymczak, and Chang Run-Hwa, Proceedings of the 1962 Annual International Conference on High Energy Physics at Geneva (CERN Scientific Information Service, Geneva, Switzerland, 1962), p. 425.

²⁶ R. Cohen, S. Devons, and A. Kanaris, Bull. Am. Phys. Soc. **8**, 26 (1963).

NE 213 (density=0.88 g/cc, composition= $\text{CH}_{1.2}$) is roughly 4 in. In measuring the proton response function, a thin detector, in which multiple collision events are improbable, should be used. Otherwise, the observed response function contains an implicit dependence on detector geometry and initial neutron direction.

A glass cylinder $\frac{1}{2}$ in. thick and 4 in. in diameter was filled with oxygen-free NE 213 and oriented coaxially with the neutron beam direction; it was viewed by a 5-in. phototube (EMI 9530B) in direct contact with the 4-in. face. The detector was placed at the end of a helium pipe 100 m from the source of a pulsed neutron beam. The beam is obtained by deflecting the cyclotron proton beam into a target once every cyclotron cycle (1/60 sec). The uncertainty in the neutron production time is at the very worst four proton rotation times, or about 200 nsec. The use of "time-of-flight" techniques permits the convenient measurement of neutron energy and the elimination of gamma-ray background. Pulses obtained directly from the phototube were displayed on an oscilloscope and photographed. The oscilloscope was triggered by the beam deflection pulse; neutron time of arrival was measured from the time of arrival of gamma rays. The pulse-height output was calibrated using the Compton recoils from gamma-ray sources of known energy, and checked with cosmic rays traversing the detector parallel to the cylinder axis (being minimum ionizing they leave a calculable amount of energy in the detector).

C. Data Taking

About 4000 photographs of the oscilloscope sweep displaying a 6- μ sec interval after gamma-ray arrival time comprised the data. Additional data of higher statistical accuracy were taken using a 400-channel RIDL pulse-height analyzer (PHA) which was triggered on selected neutron flight times. Compton recoil pulses from Co^{60} (1.25 MeV) and Na^{24} (1.38 and 2.76 MeV) gamma-ray sources were photographed and displayed on the PHA to set the energy scale. Pulses from cosmic-ray particles traversing the detector within 10° of the vertical were recorded and compared with radioactive source data. The cosmic-ray pulses served as an absolute calibration of pulse height. This was considered preferable to complete dependence on Compton recoils which are subject to detector edge effects and complications due to the Compton "edge." Space-charge saturation in the photomultiplier was avoided by requiring that the two "edges" of the Na^{24} source retain their proper pulse-height relationship as the photomultiplier voltage was raised to at least 150 V above its normal operating point of 1200 V.

The limitation in neutron-energy resolution was due to jitter of the neutron starting time (0.2 μ sec); the time interval measurement on the film was considerably more precise than this. The film yielded a flight time and pulse-height coordinate for each neutron event measured. The time scale was divided into subintervals

and the pulse-height spectrum for each of these was plotted.

A good approximation to the shape of the proton response function below 6 MeV is $R(E)=AE+BE^2$, where E is proton energy in MeV, and A and B are parameters to be determined. The analogous response to electrons is $R_e(E)=E$. On the basis of the above approximate response curve the expected proton-recoil pulse-height spectrum due to a single neutron collision is

$$\begin{aligned} N(\epsilon) &= (1/E_0)(A^2+4B\epsilon)^{-\frac{1}{2}} & \epsilon < AE_0+BE_0^2, \\ N(\epsilon) &= 0 & \epsilon > AE_0+BE_0^2. \end{aligned}$$

E_0 is the initial neutron energy and ϵ is the pulse height as compared to a Compton recoil pulse.

If monoenergetic neutrons are available, there are two ways to deduce A and B from the recoil spectrum. One is to fit the spectrum shape. An equally accurate but simple approach is to determine the end point of the spectrum ($\epsilon=AE_0+BE_0^2$) for several values of initial neutron energy E_0 . Since the proton recoil spectrum is rather flat at the upper energy end, especially for high initial neutron energies, the end point can be easily determined despite the finite pulse height resolution of the detector system.

D. Conclusion

Figure 7 shows the response curve obtained in the present experiment as well as the curves obtained by other workers. Our measurement agrees rather well with the curve used by Brooks.¹⁵ A fit to the data points yields the following response function:

$$\begin{aligned} R &= 0.28E + 0.033E^2 & E < 6 \text{ MeV}, \\ R &= 0.70E - 1.33 & E > 6 \text{ MeV}. \end{aligned}$$

In the muon capture experiment the energy threshold that was used was above the steeply rising portion of the spectrum. Neutron degradation in the hydrogen target and subtraction of accidental events as well as iron capture neutrons tended to increase the uncertainty in the low-energy end of the pulse-height spectrum decreasing sensitivity to the response curve. Nevertheless, verification of the muon-capture neutron energy (expected to be 5.2 MeV) was gratifying and was essential to correct normalization of the pulse-height spectrum. The Monte Carlo detector efficiency calculation summed the single-collision proton recoil responses to provide the correct pulse-height response in the case of multiple neutron collisions in the detector. As an additional check one of the full-sized neutron detectors used in the muon capture experiment was exposed to the monoenergetic neutron beam and its pulse-height response was compared to the predictions of a Monte Carlo calculation carried out for that situation. Agreement was found but only response data taken with thin detectors was useful in the detailed analysis of the experiment.

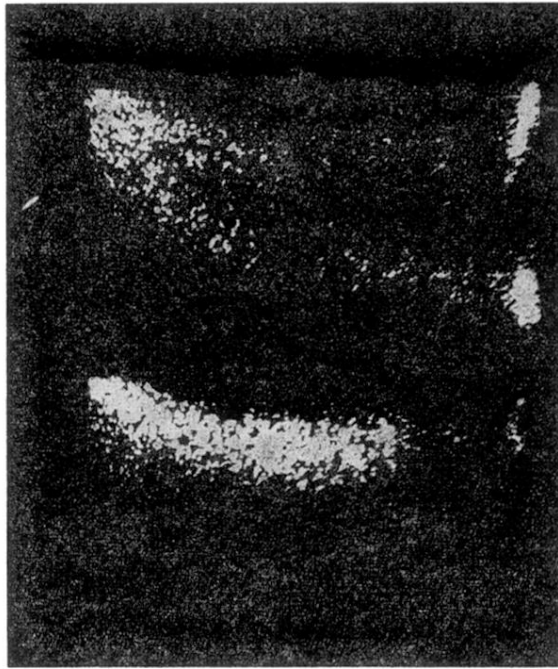


FIG. 8. Photograph of oscilloscope display of neutron and gamma-ray pulse height versus slow component residue. Horizontal axis is energy, increasing toward the right. The neutron residue is displayed on the vertical axis increasing downward. Upper photograph shows gamma ray and neutron "bands" due to a Pu-Be source. Lower picture is "band" due to a pure gamma-ray source (Cs^{137} -0.67 MeV).